Journal of *Marine Science and Engineering*

MDPI

Article

Numerical Study of Slamming Loads on Bow Flare of FPSO Model by Irregular Waves

Young Jun Kim [1], Kyong-Hwan Kim [1], Bo Woo Nam [2], Sa Young Hong [1] and Yoon-Jin Ha [1,*]

[1] Korea Research Institute of Ships and Ocean Engineering, Daejeon 34103, Republic of Korea; yjkim@kriso.re.kr (Y.J.K.); kkim@kriso.re.kr (K.-H.K.); sayhong@kriso.re.kr (S.Y.H.)
[2] Department of Naval Architecture and Ocean Engineering, Seoul National University, Seoul 08826, Republic of Korea; bwnam@snu.ac.kr
* Correspondence: yj_ha0811@kriso.re.kr

Abstract: Numerical studies were performed to investigate bow flare slamming loads under irregular waves. To estimate the slamming forces in the simulations, two time windows were selected based on existing experimental data. This study examined horizontal and vertical slamming phenomena by analyzing the relationship between the motions and the resulting slamming forces. The horizontal and vertical slamming forces from the simulations were directly compared with the experimental data. Furthermore, the experiment and simulation results were compared against a representative classification code for additional validation. The findings provide insights into the physical phenomena of horizontal and vertical slamming and confirm that the formulation suggested by classification societies provides a reasonable estimation of slamming loads. Finally, the results emphasize that both horizontal and vertical slamming forces are significant design parameters.

Keywords: CFD; irregular wave; horizontal slamming; vertical slamming; ship motion

check for updates

Academic Editor: Joško Parunov

Received: 9 January 2025
Revised: 6 February 2025
Accepted: 9 February 2025
Published: 27 February 2025

Citation: Kim, Y.J.; Kim, K.-H.; Nam, B.W.; Hong, S.Y.; Ha, Y.-J. Numerical Study of Slamming Loads on Bow Flare of FPSO Model by Irregular Waves. *J. Mar. Sci. Eng.* **2025**, *13*, 455. https://doi.org/10.3390/jmse13030455

Copyright: © 2025 by the authors. Licensee MDPI, Basel, Switzerland. This article is an open access article distributed under the terms and conditions of the Creative Commons Attribution (CC BY) license (https://creativecommons.org/licenses/by/4.0/).

1. Introduction

Local damage to ships and offshore platforms can be caused by wave forces. Therefore, both the structural safety and the hydrodynamic performance of ships and offshore platforms must be validated during the design phase. Wave slamming forces are particularly significant and frequently occur due to ever-present waves, and they can potentially cause fatigue damage to ships and offshore platforms. Slamming forces can be classified into two types based on their direction of action: horizontal slamming forces and vertical slamming forces.

In order to estimate the slamming force, various approaches using analytic solutions were initially applied to water impact problems, such as the von Karman theory [1] and the Wagner approach [2]. These analytic solutions remain widely used to estimate the slamming force for simple structures. Hermundstad and Moan [3] performed experimental analyses by installing two slamming force panels on the bow flare of a Ro-Ro vessel to investigate slamming impact forces in regular oblique waves. The test results were directly compared with a slamming calculation program based on the Wagner formulation [4], emphasizing the necessity of accurately estimating roll motion in numerical analyses.

Similar experimental and numerical studies on ship slamming include those of Wang and Soares [5], who conducted an experimental and numerical investigation of slamming loads on the bow of a chemical tanker in irregular waves, focusing on slamming occurrence probability and load distribution. Jiao et al. [6] performed theoretical and experimental analyses of nonlinear hydroelastic responses and slamming loads of a ship advancing in

regular waves, highlighting the importance of flare slamming and green water on deck. Li et al. [7] carried out an experimental study on stern slamming and the global response of a large cruise ship in regular waves, employing a segmented model test to evaluate measurement uncertainties.

Kapsenberg and Thornhill [8] measured the pressure on the bow segment of a ferry-type vessel in irregular waves by installing numerous pressure sensors on the bow section. They also conducted a CFD (Computational Fluid Dynamics) study, directly comparing the CFD results with the experimental data. Furthermore, they tried to refine the momentum theory using measured forces on the bow segment from both experiments and CFD analyses. Kim et al. [9] studied the bow slamming load in regular and irregular wave conditions using a segmented model. Also, they attempted to simplify the slamming force estimation using wedge-shape solutions. Voogt and Buchner [10] conducted a series of model tests on a ship-type Floating Production Storage and Offloading (FPSO) model, focusing on the local steepness of incoming waves. They described the relationship between the magnitude of slamming forces and wave steepness characteristics. Xu et al. [11] studied slamming impact characteristics on the bow sections of two FPSOs by using numerous pressure sensors and load cells. This study has confirmed the correlation between slamming loads and wave steepness.

Both model tests and CFD approaches are widely applied in slamming studies. Many researchers have performed drop simulations as representative slamming studies. For instance, the relationship between slamming pressures and deadrise angles has been extensively studied [12–14]. Khayyer and Gotoh [15] calculated the slamming impact pressures on a vertical wall using a modified Moving Particle Semi-Implicit Method. This study included air compressibility in estimating slamming impact pressures and highlighted improved accuracy and stability of the pressure field. Chen and Chen [16] investigated bow and stern slamming forces on a container ship using CFD. Their study showed that the free surface captured by the Level-Set Method can be used for slamming simulations. Seo and Jeong [17] compared bow flare slamming loads from CFD simulations with those from ship classification society rules and confirmed that the slamming pressures were similar. Lee et al. [18] presented an integrated experimental and numerical study on the structural response of Deep-V planning-hull grillage panels through slamming loads in irregular waves. This study highlighted the importance of capturing wave impact patterns and validating simulations for effective structural optimization.

As a fundamental study on slamming phenomena, CFD simulations were conducted to investigate the slamming characteristics of an FPSO model. In the simulation, six-degree-of-freedom (6-DoF) motions and force measurements at 15 locations were extracted and directly compared with existing experimental data [19]. Finally, the both horizontal and vertical slamming load were compared with the classification code.

2. Model and Environmental Condition

2.1. Model

The experimental model used in this study is a ship-type FPSO model, as shown in Figure 1. The main particulars of the FPSO are summarized in Table 1. A series of model tests were conducted in the KRISO ocean engineering basin. The model had a scale ratio of 1:50, and the bow of the experimental model was made of FRP.



Figure 1. FPSO experimental model.

Table 1. Main particulars of the FPSO.

Item	Prototype	Model
Length Between Perpendiculars	306.7 m	6.134 m
Breadth	58.8 m	1.176 m
Depth	27.2 m	0.544 m
Draft	16.0 m	0.320 m
Displacement Volume	abt. 200,000 m^3	abt. 1600 m^3
C_B	0.802	
Roll resonance period	14.28 s	2.02 s
Pitch resonance period	13.09 s	1.85 s

A total of 15 force sensors were used to measure the slamming force, arranged in an orderly arrangement on the bow flare area. Figure 2 illustrates the cross-sectional view of sensor installation and the force sensors' arrangement. To ensure secure installation, an aluminum frame was added inside the bow section of the model. The force sensors, KISTLER 4576A, were equipped with a 50 mm diameter force plate specifically designed to maintain the curvature of the bow. Watertight integrity between the model hull and the force plates was ensured using a watertight film. The sampling rate of the force sensor was 20 kHz. The 6-DOF motions of the model were captured using a Rodym non-contact optical motion tracking device.

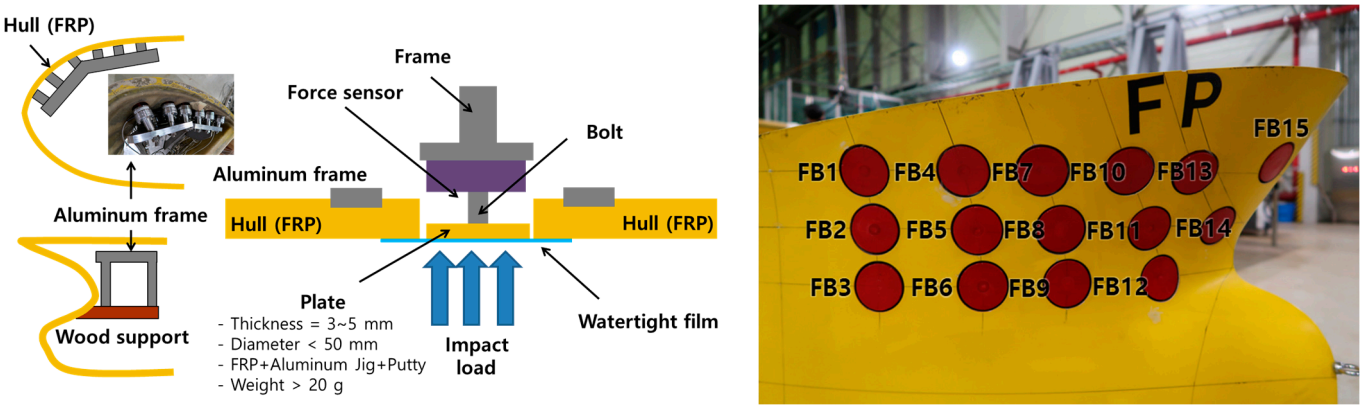

(**a**) (**b**)

Figure 2. Configuration of sensors: (**a**) cross-sectional view of the force sensor installation; (**b**) arrangement of force sensors (FB1–FB15) installed on the bow flare of the FPSO.

2.2. Environmental Condition

Initially, the model tests were conducted under regular and white noise test (WNT) wave conditions to examine the general motion characteristics of the FPSO. The motion Response Amplitude Operators (RAOs) of the FPSO are presented in Figure 3 at the prototype scale. The experimental results were directly compared with those obtained from the frequency domain analysis, referred to as AdFLOW. As shown in Figure 3, the results from the model tests exhibit good agreement with the frequency domain analysis. For roll and pitch rotational motions, the resonance frequencies are approximately 0.44 rad/s (T = 14.28 s) and 0.48 rad/s (T = 13.09 s), respectively.

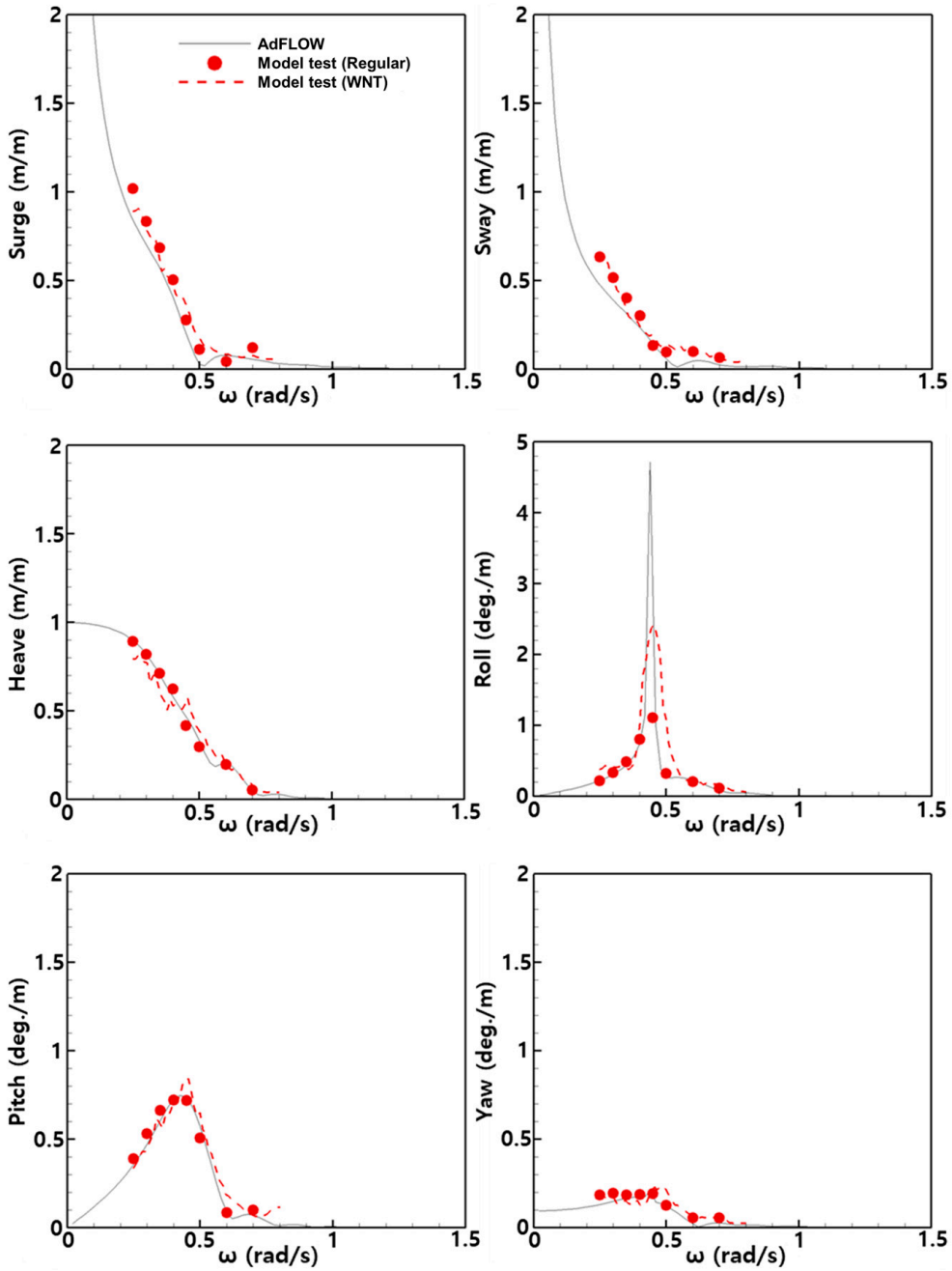

Figure 3. Comparison of FPSO motion RAOs at prototype scale.

The peak period of the irregular wave was determined to be 12.66 s, which is close to the roll and pitch resonance periods of the model, as shown in Figure 4. To generate a large slamming force, the significant wave height of the irregular wave was set at 110% of the model's freeboard. During the model tests, the displacement of the wave maker was directly measured using a laser sensor and was utilized to conduct the numerical simulations.

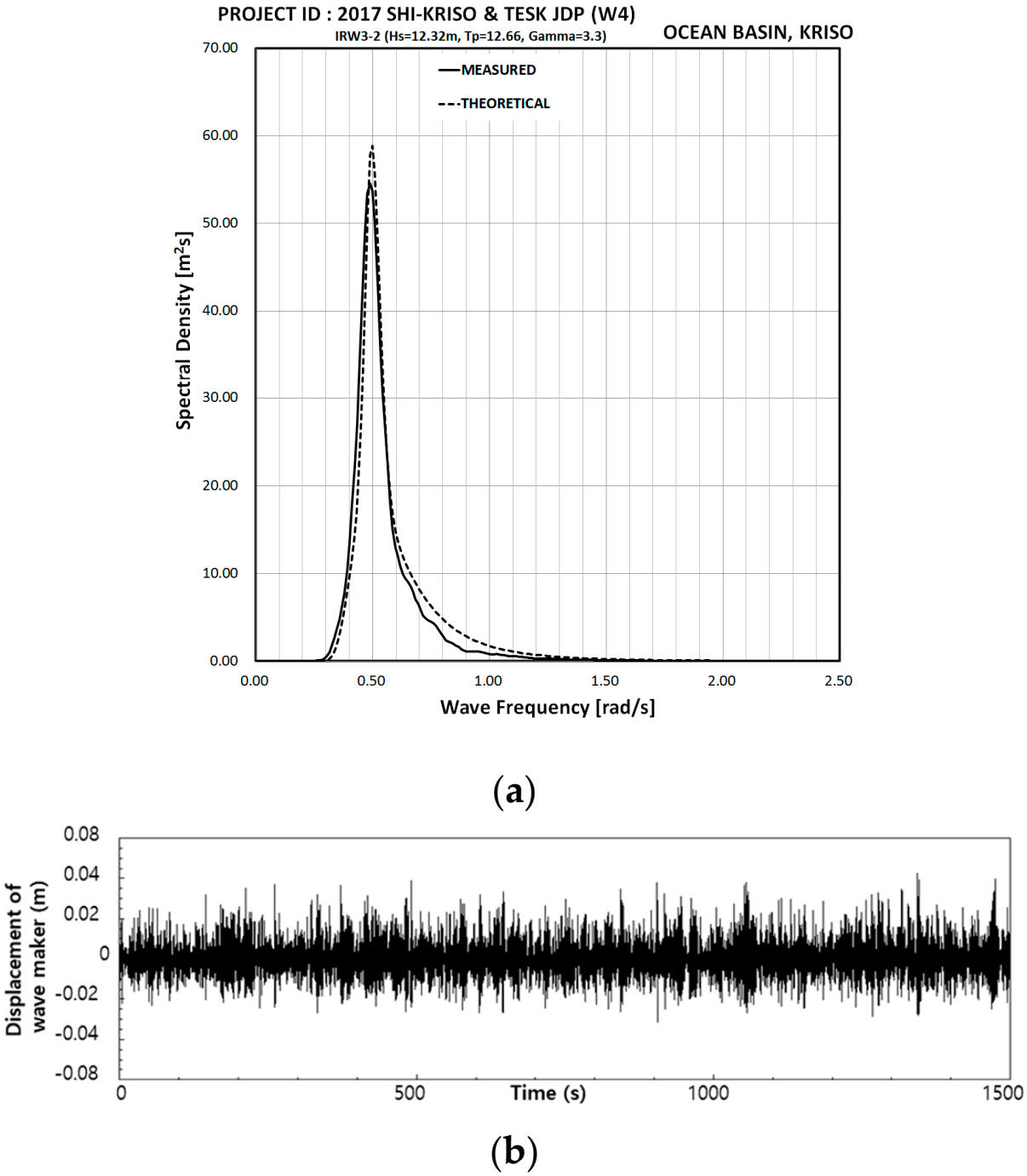

Figure 4. (**a**) Wave spectrum at prototype scale (Hs = 12.32 m, Tp = 12.66 s); (**b**) displacement of the wave maker.

3. Numerical Model

3.1. Numerical Scheme

For the numerical simulations, the commercial CFD software STAR-CCM+ (Version 11.06) was used. Table 2 summarizes the numerical schemes used in this study. The simulation was performed in model scale, and all subsequent analyses were also conducted in model scale. The second-order Upwind scheme and the second-order Euler Implicit Method were employed for the convection and time integration schemes, respectively. The time step was set to 0.005 s, determined based on the relationship between the minimum grid size and the wave velocity (CFL = 0.5).

Table 2. Numerical scheme for the numerical simulations.

Numerical Schemes	
Discretization scheme	FVM (Finite Volume Method)
Pressure and velocity field	SIMPLE (Semi-Implicit Method for Pressure Linked Equations)
Time step	0.005 s
Inner iterations	10
Convection schemes	2nd order Upwind
Time integration scheme	2nd order Euler Implicit

3.2. Grid System and Boundary Conditions

The computational domain's length and depth were set to 56 m and 3.2 m, respectively, matching the dimensions of the KRISO ocean engineering basin. To reduce the total number of grids, the domain's breadth was set to 12 m, approximately 40% of the basin's total breadth.

Figure 5 illustrates the mesh system and the boundary conditions used for this numerical study. Two refinement zones were applied: one near the free-surface region for accurate wave generation of the incoming irregular waves and the other near the relatively denser zone near the bow section for precise measurement of the slamming forces acting on the model's bow. In the numerical simulations, a damping zone of 15.0 m was implemented, corresponding to the length of the experimental wave absorber. The total number of cells used in this study was approximately 5 million.

As illustrated in Figure 5, the inlet boundary was set as a velocity inlet, the side and bottom boundaries were modeled as walls, the top boundary was defined as symmetry, the outlet boundary was assigned as a pressure outlet, and the FPSO model itself was defined as a wall. The wave maker velocity, which is a time derivative of the wave maker displacement measured during the model tests (shown in Figure 4), was applied to the inlet boundary. Additionally, four 100 kgf/m linear springs were installed to the bow and stern of the model, matching the mooring settings used in the experimental tests.

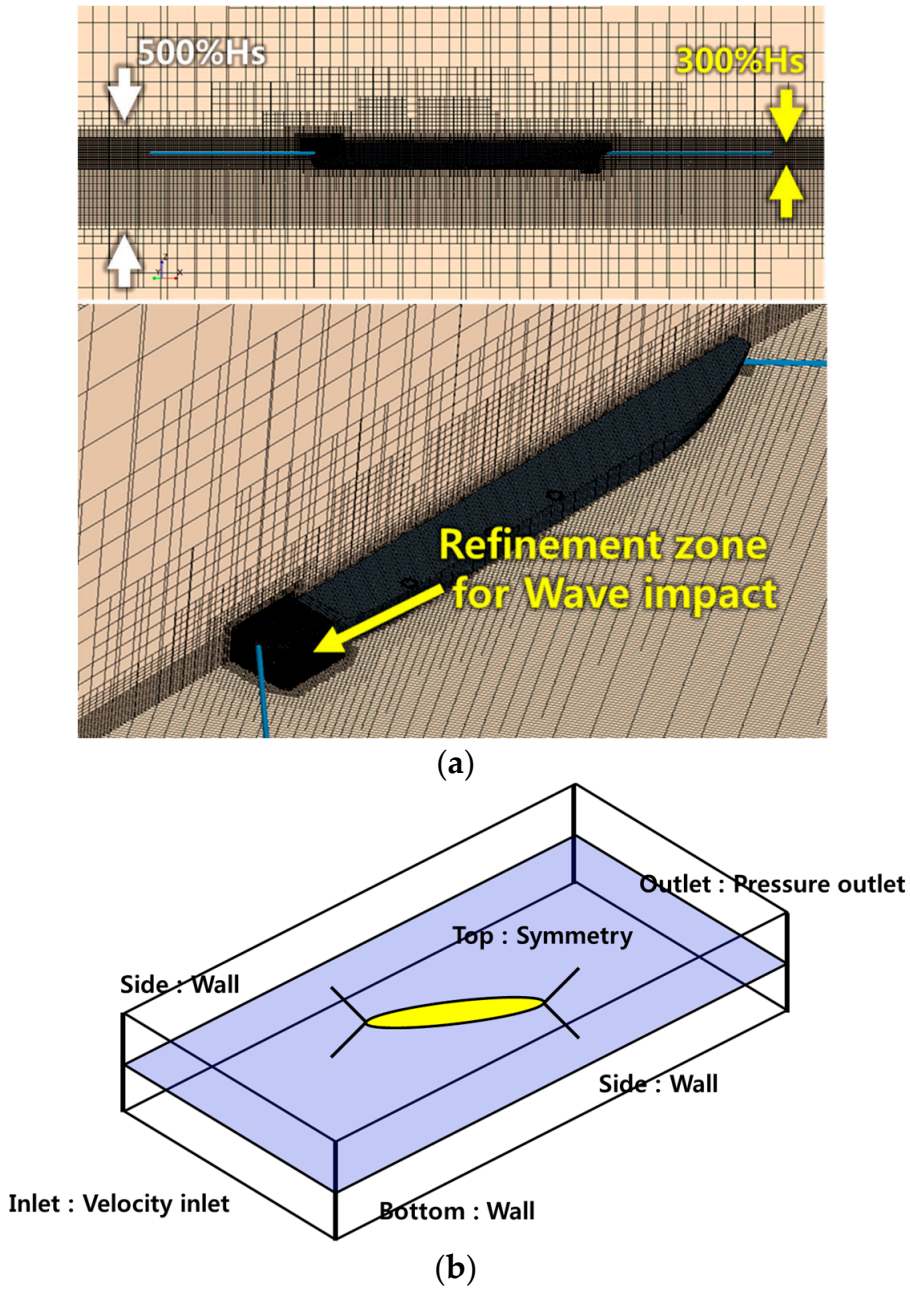

Figure 5. (**a**) Mesh and (**b**) boundary conditions for the numerical simulations.

3.3. Selction of Simulation Time Window

Figure 6 presents the experimental results, including the time histories of the 6-DOF motions and the slamming forces. In the model tests, high slamming forces were predominantly observed at the FB13, FB14, and FB15 locations. Therefore, this study focused exclusively on the slamming forces at these three force sensor results.

Relatively high slamming forces were observed when the lateral and vertical motions were significant, as shown in Figure 6. To investigate the horizontal and vertical slamming phenomena, two time windows of 100 s were selected from the model test results, and each time window is highlighted in the blue and red boxes in Figure 6.

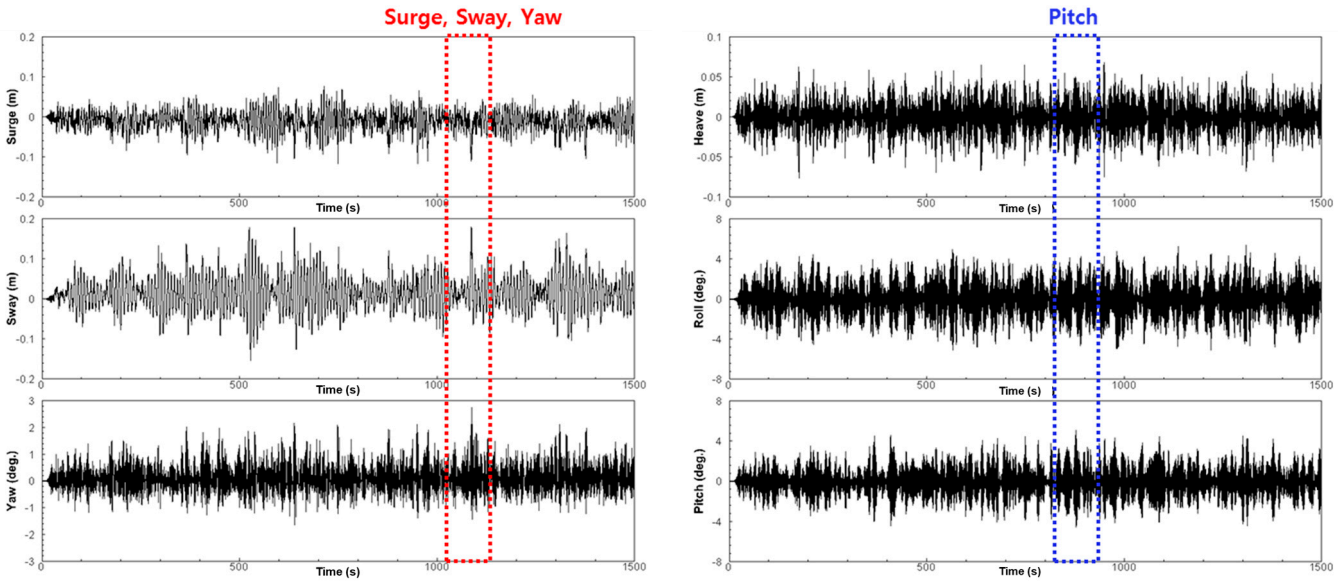

(**a**)

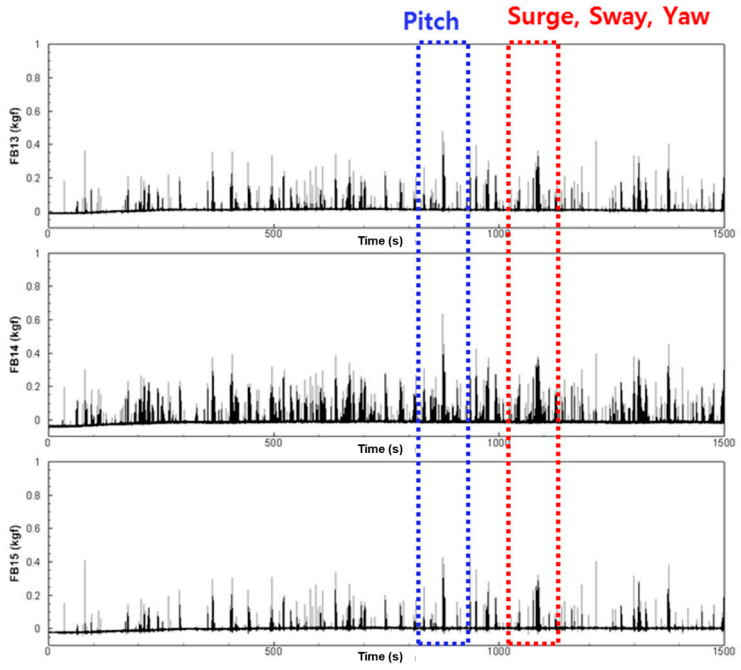

(**b**)

Figure 6. Time histories of the motions of the model and the representative slamming forces: (**a**) 6-DoF motions of the model; (**b**) corresponding time histories of the slamming forces.

4. Results and Discussions

4.1. Horizontal Slamming Force

The simulations were performed during the first time window (blue box of Figure 6) when the lateral motion was relatively large. Figure 7 shows snapshots of the experiment and simulation at the same time intervals. As shown in the figure, the bow is exposed as the wave crest approaches. Subsequently, the wave crest impacts the bow section of the FPSO as the bow moves downward due to the pitch motion. Finally, the incoming wave passes by the bow section. It is shown that the wave patterns in the numerical simulations are similar to those in the experimental snapshots.

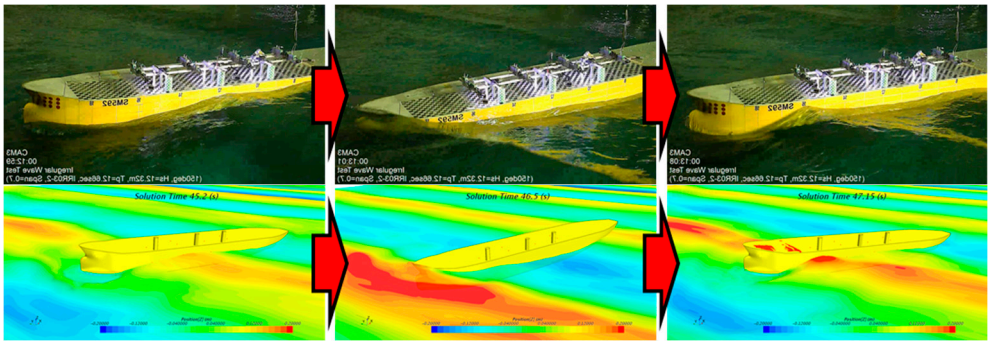

Figure 7. Snapshots of waves near the model.

In Figure 8, the motion responses and slamming forces from the simulations are compared with the model test results at model scale. The numerical simulation results show good agreement with the experimental data. Between 1070 s and 1100 s of simulation time, large slamming forces were observed especially at FB14, coinciding with significant lateral motions of the model.

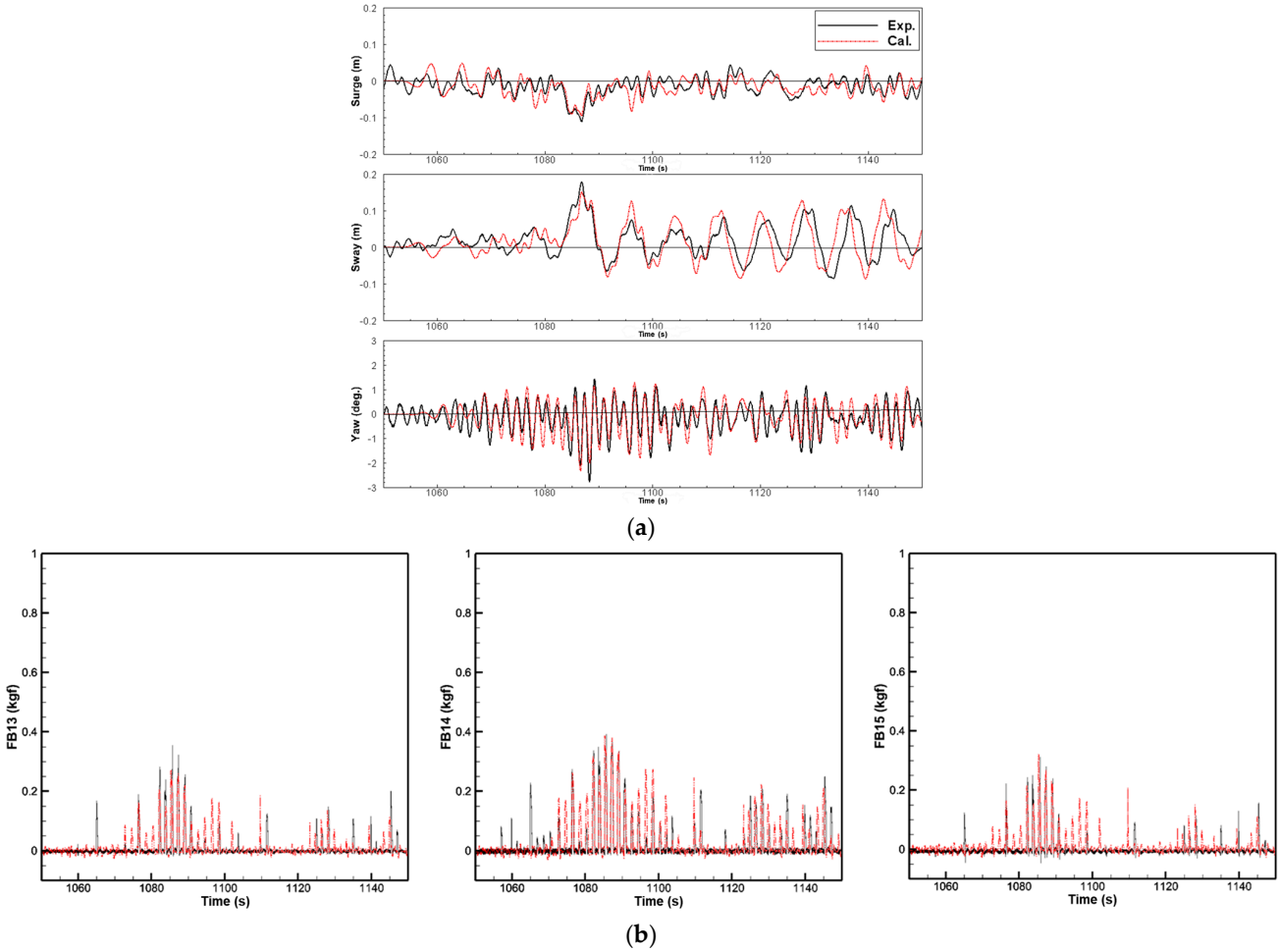

Figure 8. Comparisons of the time histories of (**a**) lateral motions and (**b**) slamming forces.

Figure 9 presents representative snapshots of the wave propagation near the bow section when a large slamming force acts on FB14. As shown in Figure 9, the incoming wave rises prominently in front of the model, and it can be observed that the high wave crest continuously collides with the bow section of the model.

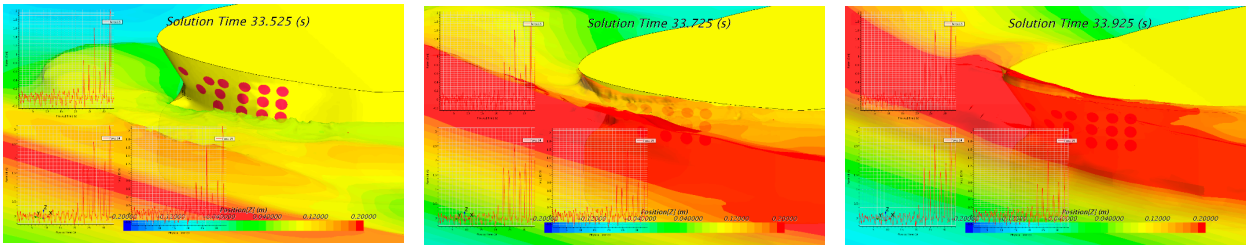

(**a**) t = 1083.525 s to 1083.925 s, Δt = 0.2 s

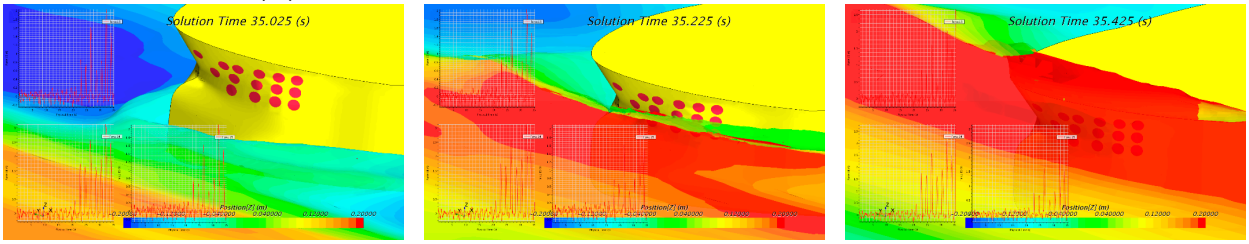

(**b**) t = 1085.025 s to 1085.425 s, Δt = 0.2 s

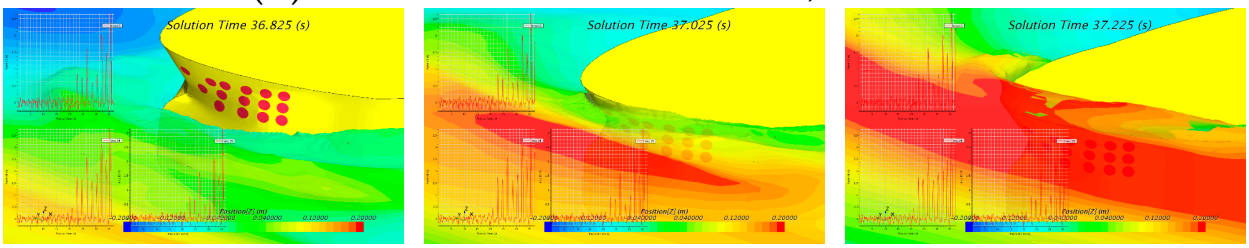

(**c**) t = 1086.825 s to 1087.225 s, Δt = 0.2 s

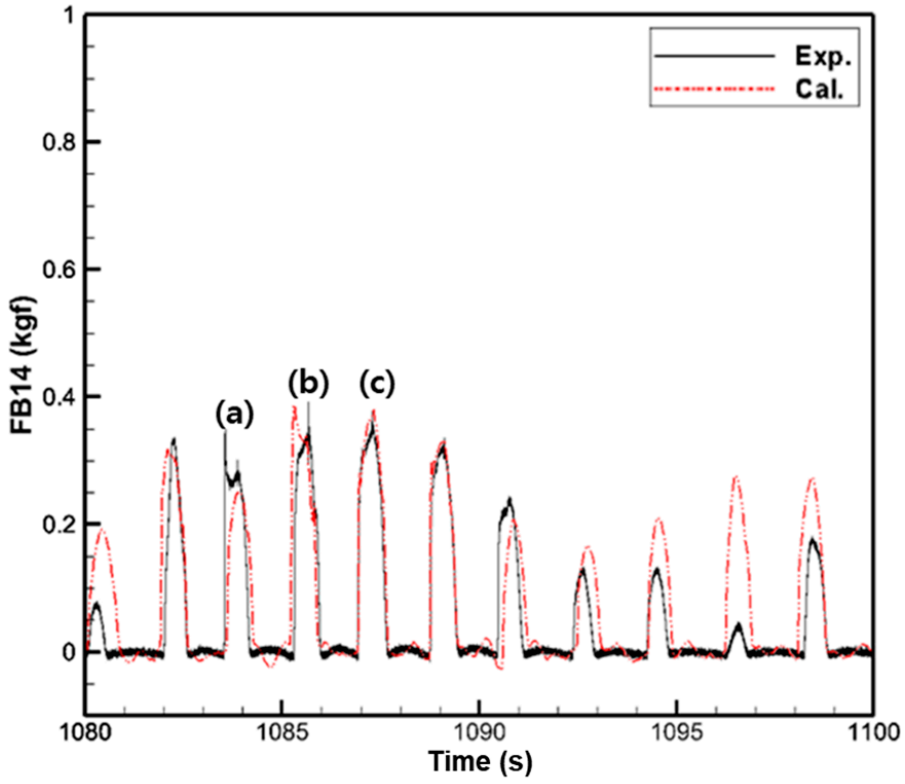

(**d**) Time histories of the slamming forces at FB14

Figure 9. (**a**–**c**) Snapshots for the wave pattern near the bow of the model and (**d**) time histories of the slamming forces at FB14 at time window (**a**–**c**).

To investigate the relationship between the motion response of the model and the slamming loads on the bow flare, Figure 10 presents the time histories of the FPSO model's motions during the same time period as Figure 9. It can be observed that three consecutive horizontal impact loads slightly push the model backward. Additionally, the sway and yaw motions of the model are induced by the wave forces under the bow quartering sea condition. In this study, the lateral motions occur in the order of sway, yaw, and surge.

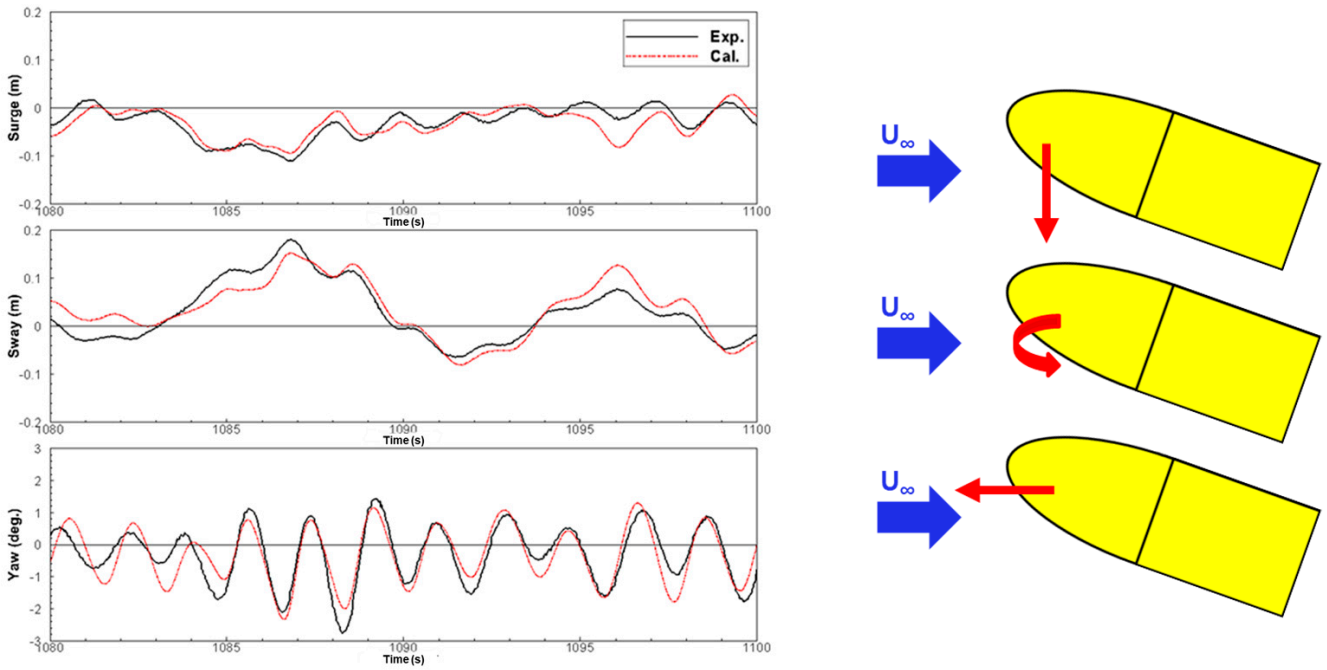

Figure 10. Cases of slamming occurrence by each lateral motion of the model.

4.2. Vertical Slamming Force

Figure 11 shows the slamming forces during the second time window, corresponding with the vertical slamming forces at the model scale. Overall, both the occurrence times and magnitudes of the impact forces show good agreement between the experimental data and the numerical simulations. Figure 12 presents snapshots of the vertical slamming phenomena. Unlike horizontal slamming, vertical slamming occurs as the bow submerges in the wave surface.

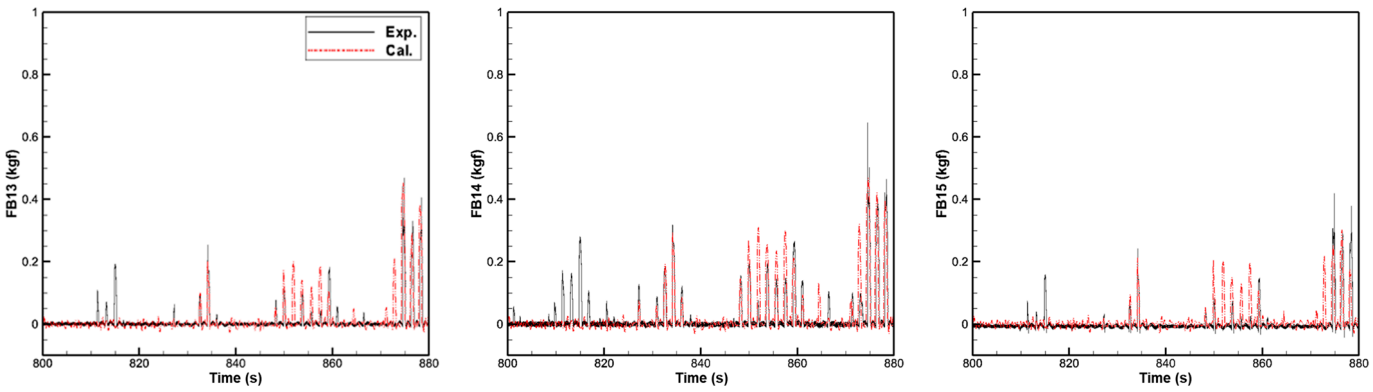

Figure 11. Comparisons of time histories for slamming forces in second time window.

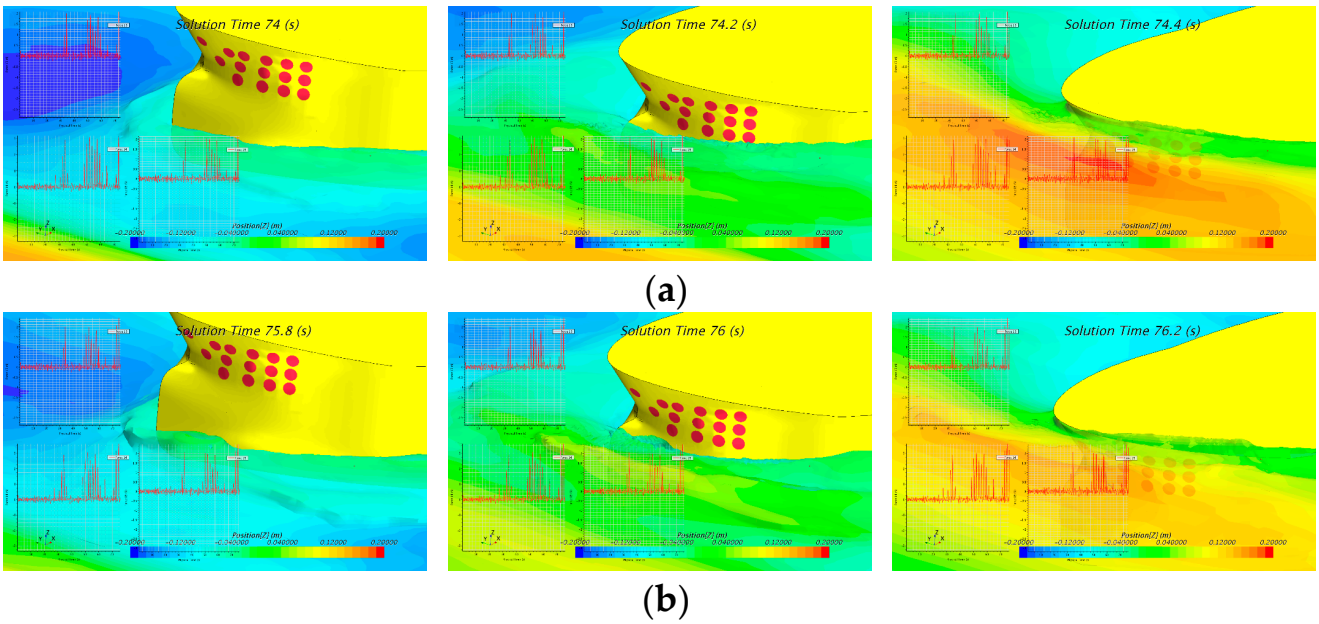

Figure 12. Snapshots for the wave pattern around the bow of the model and the time histories of the slamming forces at FB14: (**a**) t = 874.0 s to 874.4 s, Δt = 0.2 s; (**b**) t = 875.8 s to 876.2 s, Δt = 0.2 s.

As shown in Figure 13, the vertical slamming forces increase when the heave and pitch motions of the model become large simultaneously. This indicates that vertical slamming forces are mainly influenced by the heave and pitch motion responses of the model. During this period, the roll motion is relatively large, particularly between 860 s and 870 s. Interestingly, at around 861 s, the slamming forces are relatively small despite the large roll motions of the model. This implies that vertical slamming forces are predominantly affected by the heave and pitch motions rather than the roll motion. As shown in Figure 14, the contribution of roll motion to slamming forces appears to be minimal. Therefore, significant vertical slamming forces are expected under head sea conditions.

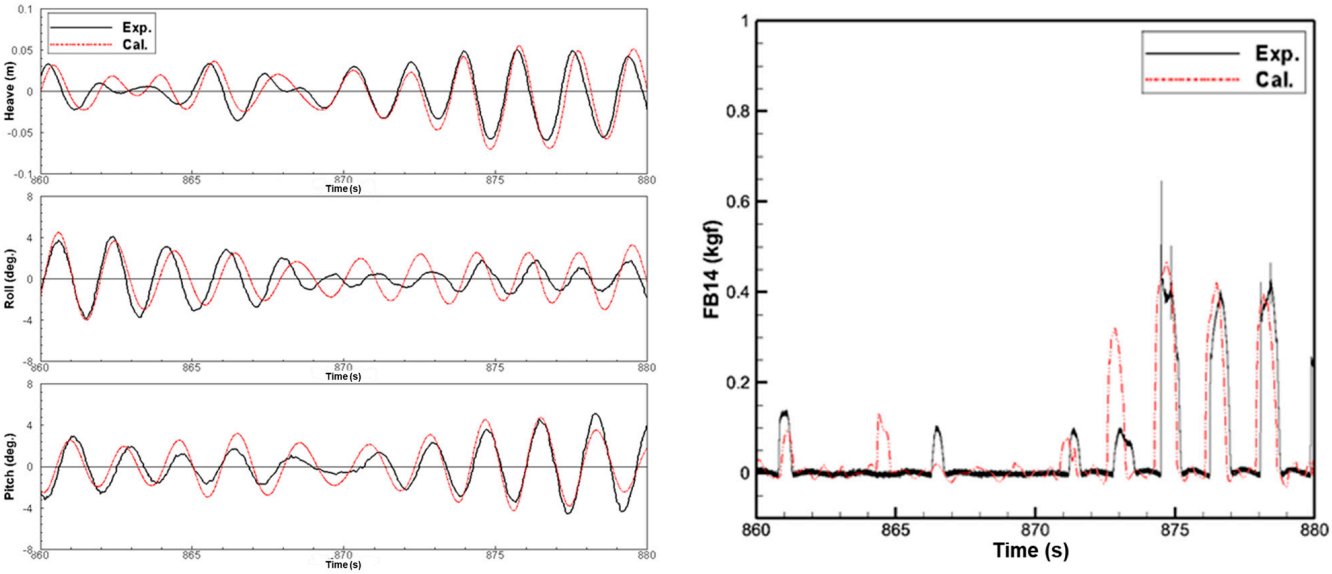

Figure 13. Relations between the vertical motions and the wave impact forces.

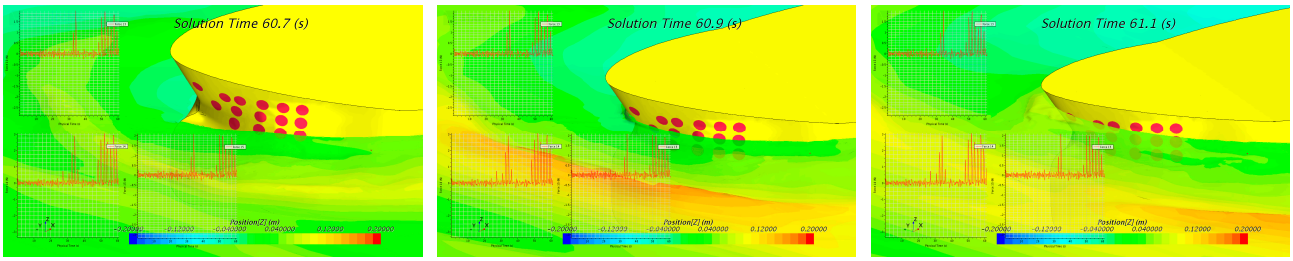

Figure 14. Snapshots of the wave propagation near the bow flare (t = 860.7 s to 861.1 s, Δt = 0.2 s).

In terms of magnitude, the largest horizontal slamming force is comparable to the largest vertical slamming force, as seen in Figures 8 and 11. Therefore, both vertical and horizontal slamming forces can be considered as significant design parameters during the design phase.

4.3. Comparisons with Slamming Forces by Rule

For an additional validation, the representative classification code suggested by classification societies was utilized in this study. Seo et al. [20] calculated the slamming forces on the bow flare of a containership using various classification codes, including ABS [21], DNV-GL [22], LR [23], and KR [24]. Their results indicated that among compared classification societies, the wave impact pressure from LR showed the best match with the experimental results.

The LR classification code is expressed as Equation (1), where K_{bf} is the hull form shape coefficient for wave impact and K_{rv} is the hull form shape coefficient for impact due to forward speed. These parameters are associated with the effective deadrise angle and buttock angle measured in the longitudinal plane, respectively. In the equation, V_{bf} represents the wave impact velocity, and V_{rv} is the relative forward speed. The wave impact velocity can be calculated based on the buttock angle, while the velocity from the surge motion shown in Figure 6a was applied to determine the relative forward speed. For the heading effect, the relative wave heading coefficient H_{rv} was considered.

$$P_{bf} = 0.5\left(K_{bf}V_{bf}^2 + K_{rv}H_{rv}V_{rv}^2\right) \text{ kN/m}^2 \quad (1)$$

To compare the experimental, numerical results, and the classification code, the maximum slamming forces at the FB13, FB14, and FB15 locations were selected from both the experimental and numerical results. For the horizontal slamming force, the maximum occurred at approximately 1085.5 s (Figure 9b), while the maximum vertical slamming force occurred at around 875 s (Figure 12b). The relative forward speed V_{rv} in Equation (1) was estimated using motion data from the experimental and simulation results at the moments when the maximum slamming forces occurred.

Figure 15 illustrates the comparison of slamming forces among the experimental results, numerical results, and the LR classification code. For the classification code results, the estimated slamming pressures were converted into slamming forces using the force panel diameter. In general, the experimental and numerical results show good agreement with the estimated slamming forces from the classification code. Since most waves in the irregular wave conditions were non-breaking, the uncertainty in wave velocity was small, which likely contributed to the favorable agreement. These results indicate that the classification code is a relatively useful method for estimating slamming loads during the design phase. Additionally, the results show that the magnitudes of both the horizontal and vertical slamming forces are similar, confirming that both forces are important parameters from a design perspective.

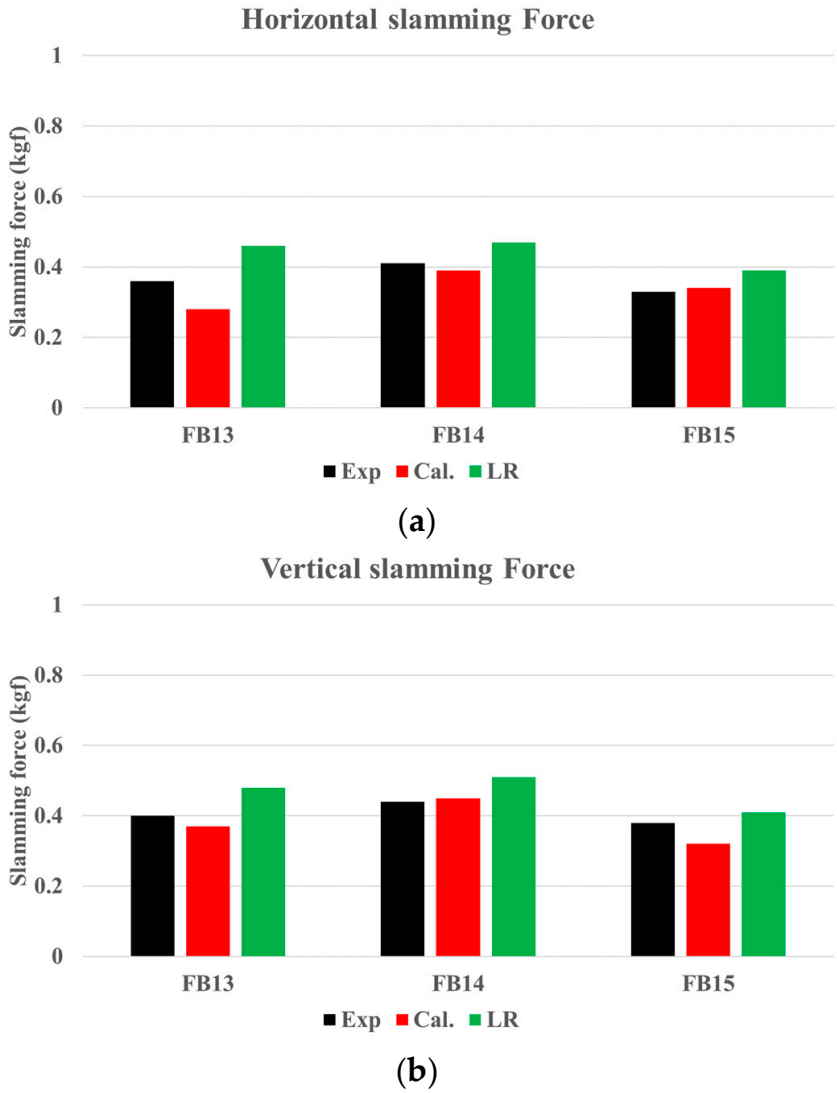

Figure 15. Comparisons for the maximum slamming forces: (**a**) horizontal slamming force; (**b**) vertical slamming force.

5. Conclusions

In this study, numerical simulations were conducted on an FPSO model to investigate the horizontal and vertical slamming forces under irregular wave conditions.

- The simulation results show good agreement with the experimental results, indicating that simulations can be effectively used as a design tool. In this study, horizontal slamming occurred consecutively as a result of the lateral motions of the model. Large vertical slamming forces were caused by the heave and pitch motions, while the contribution of roll motion to vertical slamming forces was relatively small. The results suggest that large vertical slamming forces could occur under head sea conditions.
- Regarding the magnitude of slamming forces, the largest horizontal slamming force and the largest vertical slamming force were found to be of similar magnitude in this study. This indicates that both horizontal and vertical slamming forces should be considered as significant design parameters during the structural design phase.
- The model tests and simulations were conducted under non-breaking wave conditions, where the uncertainty in wave velocity was small. Under these conditions, the experimental and numerical results showed good agreement with the representative

classification code. This result also indicated that the classification code is a useful tool for the initial design of the bow of an FPSO.

- In the future, it will be necessary to investigate horizontal and vertical slamming forces through numerical simulations under other wave headings. Such studies could provide more meaningful insights for the optimal design of the bow.

Author Contributions: Conceptualization, Y.-J.H., Y.J.K., K.-H.K., S.Y.H. and B.W.N.; methodology, Y.-J.H. and Y.J.K.; validation, Y.-J.H. and Y.J.K.; writing—original draft preparation, Y.-J.H. and Y.J.K.; writing—review and editing, Y.-J.H., Y.J.K., K.-H.K., S.Y.H. and B.W.N.; visualization, Y.-J.H.; supervision, K.-H.K., S.Y.H. and B.W.N.; funding acquisition, K.-H.K., S.Y.H. and B.W.N. All authors have read and agreed to the published version of the manuscript.

Funding: This study was supported by grants from the Korea Institute of Marine Science & Technology Promotion (KIMST) funded by the Ministry of Oceans and Fisheries (RS-2022-KS221682) and supported by the Korea Research Institute of Ships and Ocean Engineering and through a grant from the Endowment Project of "Development of core technology for offshore green hydrogen to realize a carbon-neutral society" funded by the Ministry of Oceans and Fisheries (2520000286).

Institutional Review Board Statement: Not applicable.

Informed Consent Statement: Not applicable.

Data Availability Statement: Data are contained within the article.

Conflicts of Interest: The authors declare no conflicts of interest.

References

1. Von Kármán, T. The Impact on Seaplane Floats during Landing. *Natl. Advis. Comm. Aeronaut. Tech. Notes* **1929**, 1–8.
2. Wagner, H. Über Stoß-Und Gleitvorgänge an Der Oberfläche von Flüssigkeiten. *ZAMM—J. Appl. Math. Mech./Zeitschrift Angew. Math. Mech.* **1932**, *12*, 193–215. [CrossRef]
3. Hermundstad, O.A.; Moan, T. Numerical and Experimental Analysis of Bow Flare Slamming on a Ro-Ro Vessel in Regular Oblique Waves. *J. Mar. Sci. Technol.* **2005**, *10*, 105–122. [CrossRef]
4. Zhao, R.; Faltinsen, O.M.; Haslum, H.A. A Simplified Nonlinear Analysis of a High-Speed Planing Craft in Calm Water. In Proceedings of the FAST'97 Conference, Sydney, Australia, 21–23 July 1997.
5. Wang, S.; Guedes Soares, C. Experimental and Numerical Study of the Slamming Load on the Bow of a Chemical Tanker in Irregular Waves. *Ocean Eng.* **2016**, *111*, 369–383. [CrossRef]
6. Jiao, J.; Zhao, Y.; Ai, Y.; Chen, C.; Fan, T. Theoretical and Experimental Study on Nonlinear Hydroelastic Responses and Slamming Loads of Ship Advancing in Regular Waves. *Shock Vib.* **2018**, *2018*, 2613832. [CrossRef]
7. Li, H.; Zou, J.; Deng, B.; Liu, R.; Sun, S. Experimental Study of Stern Slamming and Global Response of a Large Cruise Ship in Regular Waves. *Mar. Struct.* **2022**, *86*, 103294. [CrossRef]
8. Kapseriberg, A.; Thornhill, E.T.; Kapsenberg, G.K. A Practical Approach to Ship Slamming in Waves. In Proceedings of the 28th Symposium on Naval Hydrodynamics, Pasadena, CA, USA, 12–17 September 2010.
9. Kim, K.H.; Kim, B.W.; Hong, S.Y. Experimental Investigations on Extreme Bow-Flare Slamming Loads of 10,000-TEU Containership. *Ocean Eng.* **2019**, *171*, 225–240. [CrossRef]
10. Voogt, A.; Buchner, B. Prediction of Wave Impact Loads on Ship-Type Offshore Structures in Steep Fronted Waves. In Proceedings of the 14th International Offshore and Polar Engineering Conference, Toulon, France, 23–28 May 2004.
11. Xu, L.; Barltrop, N.; Okan, B. Bow Impact Loading on FPSOs 1-Experimental Investigation. *Ocean Eng.* **2008**, *35*, 1148–1157. [CrossRef]
12. Zhao, R.; Faltinsen, O.; Aarsnes, J. Water Entry of Arbitrary Two-Dimensional Sections with and Without Flow Separation. In Proceedings of the 21st Symposium on Naval Hysdrodynamics, Trondheim, Norway, 24–28 June 1996; pp. 408–423.
13. Wang, S.; Guedes Soares, C. Analysis of the Water Impact of Symmetric Wedges with a Multimaterial Eulerian Formulation. *Int. J. Marit. Eng.* **2012**, *154*, A191–A205. [CrossRef]
14. Wang, S.; Guedes Soares, C. Slam Induced Loads on Bow-Flared Sections with Various Roll Angles. *Ocean Eng.* **2013**, *67*, 45–57. [CrossRef]
15. Khayyer, A.; Gotoh, H. Modified Moving Particle Semi-Implicit Methods for the Prediction of 2D Wave Impact Pressure. *Coast. Eng.* **2009**, *56*, 419–440. [CrossRef]

16. Chen, C.-R.; Chen, H.-C. CFD Simulation of Bow and Stern Slamming on a Container Ship in Random Waves. *Int. J. Offshore Polar Eng.* **2015**, *25*, 239–240. [CrossRef]
17. Seo, D.W.; Jeong, K.L. Numerical Study on the Prediction of the Bow Flare Slamming Pressure for the Container Ship in Regular Wave. *Brodogradnja* **2019**, *70*, 25–42. [CrossRef]
18. Lee, E.J.; Diez, M.; Harrison, E.L.; Jiang, M.J.; Snyder, L.A.; Powers, A.M.R.; Bay, R.J.; Serani, A.; Nadal, M.L.; Kubina, E.R.; et al. Experimental and Computational Fluid-Structure Interaction Analysis and Optimization of Deep-V Planing-Hull Grillage Panels Subject to Slamming Loads—Part II: Irregular Waves. *Ocean Eng.* **2024**, *292*, 116346. [CrossRef]
19. Ha, Y.-J.; Kim, K.-H.; Nam, B.W.; Hong, S.Y.; Kim, H. Experimental Study for Characteristics of Slamming Loads on Bow of a Ship-Type FPSO under Breaking and Irregular Wave Conditions. *Ocean Eng.* **2021**, *224*, 108738. [CrossRef]
20. Seo, M.G.; Nam, B.W.; Kim, K.H.; Lee, K.S.; Hong, S.Y. Study of the Bow-flare Impact Pressure on the Container ships. In Proceedings of the Annual Autumn Conference, SNAK, Yeosu, Republic of Korea, 2–3 November 2017.
21. ABS. *Slamming Loads and Strength Assessment for Vessels*; ABS: New York, NY, USA, 2011; Section 2.
22. DNV-GL. *Rules for Classification*; 2017; Part 3, Chapter 10, Section 1. Available online: https://www.scribd.com/document/507365579/DNVGL-RU-SHIP-Pt3Ch7 (accessed on 1 January 2025).
23. Lloyd's Register. *Rules and Regulations for the Classification of Ships*; 2016; Part 4, Chapter 2, Section 4. Available online: https://diving-rov-specialists.com/index_htm_files/vd_50-lloyds-rules-and-reg-clas-ships.pdf (accessed on 1 January 2025).
24. KR. *Rules for the Classification of Steel Ships*; KR: Busan, Republic of Korea, 2015; Part 3.

Disclaimer/Publisher's Note: The statements, opinions and data contained in all publications are solely those of the individual author(s) and contributor(s) and not of MDPI and/or the editor(s). MDPI and/or the editor(s) disclaim responsibility for any injury to people or property resulting from any ideas, methods, instructions or products referred to in the content.